Journal of
Marine Science and Engineering

MDPI

Article

Hydrodynamic Performance of Submerged Plates During Focused Waves

Qinghe Fang [1,2], Can Yang [3] and Anxin Guo [1,*]

1 Key Lab of Structures Dynamic Behavior and Control of the Ministry of Education, School of Civil Engineering, Harbin Institute of Technology, Harbin 150090, China; qinghefang@hit.edu.cn
2 Key Laboratory of Coastal Disasters and Defence of Ministry of Education, Hohai University, Nanjing 210098, China
3 College of Shipbuilding Engineering, Harbin Engineering University, Harbin 150001, China; cyangdlut@163.com
* Correspondence: guoanxin@hit.edu.cn

Received: 28 September 2019; Accepted: 23 October 2019; Published: 31 October 2019

check for updates

Abstract: Submerged horizontal plates are widely employed in research of wave structure interaction as a simplification of coastal and ocean engineering structures. The hydrodynamic performance of submerged horizontal plates under focused waves has been seldom reported. Based on potential flow theory, this paper presents a general solution of the hydrodynamic pressure and wave forces exerted on submerged plates by a focused wave group. An existing experiment and two limiting cases are used to validate the accuracy of the present analytical model. With the validated model, the effect of wave properties and the configuration of the wave structure system on the hydrodynamic performance of submerged plates are investigated. It is found that the hydrodynamic performance of submerged horizontal plates varies with incident focused wave with different peak frequencies. The structural breadth significantly changes the hydrodynamic performance while the structural height has little influence. This paper shows the usefulness of potential flow theory for the preliminary calculation of wave loads on coastal and ocean engineering structures generated by focused waves.

Keywords: Submerged horizontal plates; analytical solution; focused wave; wave reflection; wave forces

1. Introduction

During the service period of offshore and coastal structures, freak waves, alternatively named rogue waves or extreme waves, which have been observed in the ocean [1] and coastal zones [2] are great threats to structural safety. It is essential to have enough knowledge about the action of freak waves on structures to design reliable and economical offshore and coastal structures. Several studies were carried out by researchers and engineers to obtain insight into the freak wave structure interaction.

In the study of the freak wave-structure interaction, an important problem is how to reproduce freak waves in the laboratory or as a numerical model. As there is no well-rounded theoretical model for freak waves [3], different methods [4] to generate freak waves in wave flumes or basins were developed and implemented [5], and subsequently extended into numerical simulations [6]. The most frequently used approach is the dispersive focusing method, which employs the dispersion characteristics of water waves at different periods travelling at different speeds to gather the crest of all wave components at the target location at the same time.

With successfully generated focused waves, various studies were conducted to investigate freak wave action on structures experimentally and numerically. General structural members, such as vertical and horizontal cylinders, were examined by researchers. Wave forces generated by nonbreaking focused waves acting on a single vertical cylinder were firstly studied with incident focused waves [7]. Different orders of wave force acting on the surface-piercing column were recognized from the measured forces under different phase focused wave groups [8], and were estimated based on linear theoretical calculation [9]. Deng, et al. [10] studied freak wave forces acting on vertical cylinders by generating freak waves in a numerical wave flume based on dispersive focusing and amplitude-phase iteration. Moreover, breaking wave forces on vertical cylinders were investigated [11] by means of deterministic breaking focused waves [12]. Similar to vertical cylinders, focused wave action on horizontal cylinders was investigated with a similar approach [13–15].

Different from single structural members, focused wave action on fixed or movable floating structures is much more complex. The motion of a floating body during a focused wave group was experimentally measured in a 15 m long and 5 m wide wave flume by Weller, et al. [16]. The effect of water-on-deck during the focused wave acting on a floating body was also discussed [17]. Moreover, the response of a semi-submersible under a freak wave was investigated, taking an experimental [18] and numerical [19] approach. It was concluded that a focused wave can serve as a suitable incident wave to study the behavior of a floating body during a freak wave. By specifying complex structures such as plate breakwaters, jetties, and platforms as horizontal plates, Suchithra and Koola [20] found that the impact force generated by focused waves was larger than that of regular waves. The effect of beams under plates on wave impact was numerically addressed in another study [21]. Furthermore, the influence of structural stiffness [22], green water [23], and accompanying current [24] on freak wave action was investigated.

Submerged plates make an ideal breakwater because of their environmentally friendly features. Scientific exploration is ongoing to obtain better hydrodynamic performance of this type of structure. With the assumption of a flat seabed, wave interaction with submerged single-layer [25], double-layers [26] and multilayers [27] horizontal plates were studied experimentally and theoretically. Furthermore, the effects of wave angle, current, topography, porosity, and neighboring boundary on the wave-structure interaction were investigated [28].

Although several studies have been carried out, there are few reports about freak wave action on submerged plates. Most of the existing studies look at the hydrodynamic performance of submerged plates under regular waves; even focused waves were validated as feasible to study freak wave action on structures. The focusing method was widely adopted to generate extreme waves based on linear wavemaker theory in the scope of potential flow theory. The analytical method based on potential flow theory was successfully applied to investigate wave action on submerged plates with different layouts [28] and caissons [29] as validated by experimental results [30]. Therefore, it is reasonable to use the potential method to gain basic insights into the interaction mechanism of freak wave action on submerged plates.

In this paper, an analytical model of focused wave action on submerged plates was setup based on potential flow theory. The boundary value problem of this physical process was solved with a matching eigenfunction method. The analytical model was validated effective to investigate wave action on submerged plates by the results of three different experiments. Considering convenience and efficiency, the analytical model was employed to study the effects of wave properties and the configuration of the wave structure system on the hydrodynamic performance of submerged plates in this paper. This paper contains five parts. Section 2 reports the detailed analytical formula for the boundary value problem of focused waves acting on submerged plates. In the following section, the effect of truncation order of evanescent modes is checked, and an existing experiment and two limiting cases are presented to validate the accuracy of the present analytical model. In Section 4, the effects of wave properties and the configuration of the wave structure system on the hydrodynamic performance are discussed. Concluding remarks are provided in the conclusion.

2. Mathematical Formulations

2.1. Boundary Value Problem

A schematic of the wave structure system is shown in Figure 1. For convenience in the following analysis, a two-dimensional Cartesian coordinate system is defined with the origin on the undisturbed free surface. The z-axis of the coordinate system is assumed to be upward and the x-axis overlaps with the still water level (SWL) coinciding with the propagation of waves. A rigid plate is fixed below the free surface with submergence d_1 in the water with constant depth d. The breadth and height of the submerged plate are B and h, respectively.

The surface elevation $\eta(x,t)$ of a 2-dimensional focused wave can be expressed by a series of monochromatic waves

$$\eta(x,t) = \sum_{n=1}^{N_f} a_n cos(k_n x - \omega_n t + \phi_n) = \sum_{n=1}^{N_f} a_n cos\theta_n \tag{1}$$

where a_n, k_n, ω_n and ϕ_n are amplitude, wave number, angular frequency, and initial phase of the n-th wave component, respectively; $\theta_n = k_n x - \omega_n t + \phi_n$ is the phase; and N_f is the total number of wave components in the focused wave group. The angular frequency and wave number satisfy the water wave dispersion relation. The ϕ_n can be by determined by $cos(k_n x - \omega_n t + \phi_n) = 1$ with specified focusing time t_b and focusing location x_b.

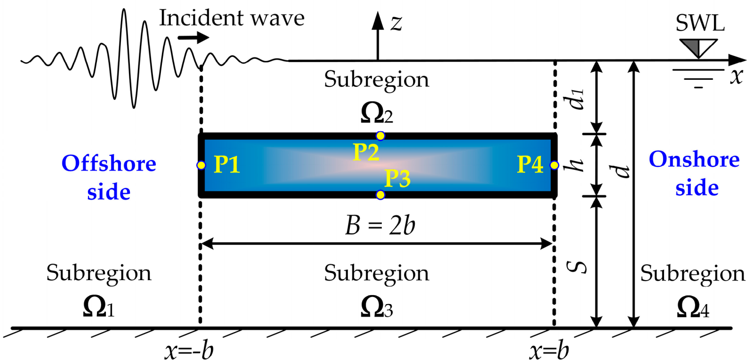

d: Water depth; d_1: Submergence; S: Water depth under the plate;
B: Structural breadth; h: Structural height.
Location: P1 ($-b$, $-d_1$-h/2); P2 (0, $-d_1$); P3 (0, $-d_1$-h); P4 (b, $-d_1$-h/2).

Figure 1. Schematic view of the wave structure system.

The elevation of the focused wave with focusing time t_b and focusing location x_b is

$$\eta(x,t) = \sum_{n=1}^{N_f} a_n \cos(k_n(x - x_b) - \omega_n(t - t_b)) \tag{2}$$

The NewWave [31,32] type focused wave is employed in this study to assign the amplitude of each wave component:

$$a_n = A_{max} S_n(\omega)\Delta\omega / \sum_{l=1}^{N_f} S_l(\omega)\Delta\omega \tag{3}$$

where $S_l(\omega)$ is the discretized energy spectrum, which is the JONSWAP spectrum [33] in the present study, $\Delta\omega$ is the frequency resolution and A_{max} is the maximum crest amplitude equal to the summation of a_n.

Treating the water as an inviscid potential flow, the velocity potential of the incident focused wave can be obtained by summing the velocity potential of each wave component:

$$\Phi(x,z,t) = \mathbf{Re}\left\{\sum_{n=1}^{N_f} \psi_n(x,z)\mathrm{e}^{-i\theta_n}\right\} \tag{4}$$

where $\psi_n(x,z)$ is the velocity potential of the n-th wave component, i is the imaginary number and **Re**{} represents taking the real part of the complex equation.

The velocity potential $\psi_n(x,z)$ of each wave component satisfies the governing Laplace equation:

$$\frac{\partial^2\psi_n(x,z)}{\partial x^2} + \frac{\partial^2\psi_n(x,z)}{\partial z^2} = 0 \tag{5}$$

and corresponding free surface, impermeable seabed, structural surface and far field conditions:

$$\begin{array}{ll} \frac{\partial\psi_n}{\partial z} - \frac{\omega_n{}^2}{g}\psi_n = 0 & (z=0) \\ \frac{\partial\psi_n}{\partial z} = 0 & (z=-d) \\ \frac{\partial\psi_n}{\partial n_S} = 0 & (on\ \Gamma_B) \\ \frac{\partial\psi_n}{\partial x} \mp ik_n\psi_n = 0 & (x \to \pm\infty) \end{array} \tag{6}$$

where g is gravitational acceleration and $\boldsymbol{n}_S$ is the outward normal vectors of the outward normal vector Γ_B.

2.2. Analytical Solutions

As shown in Figure 1, the entire fluid domain consists of four subregions with different boundary conditions: Region 1: Ω_1 ($-\infty < x < -b$, $-d < z < 0$); Region 2: Ω_2 ($-b < x < b$, $-d_1 < z < 0$); Region 3: Ω_3 ($-b < x < b$, $-d < z < -d_1 - h$); and Region 4 Ω_4 ($b < x < \infty$, $-d < z < 0$). The velocity potential for those four subregions are [34,35]:

$$\psi_n^1 = \left(e^{ik_0^1(x+b)} + A_0^1 e^{-ik_0^1(x+b)}\right)Z_0^1 + \sum_{m=1}^{\infty} A_m^1 e^{k_m^1(x+b)} Z_m^1,\ (-\infty < x < -b,\ -d < z < 0) \tag{7}$$

$$\psi_n^2 = \left(A_0^2 cosk_0^2 x + B_0^2 sink_0^2 x\right)Z_0^2 + \sum_{m=1}^{\infty}\left(A_m^2 \frac{coshk_m^2 x}{coshk_m^2 b} + B_m^2 \frac{sinhk_0^2 x}{coshk_m^2 b}\right)Z_m^2, (-b < x < b, -d_1 < z < 0) \tag{8}$$

$$\psi_n^3 = \left(A_0^3 + B_0^3 \frac{x}{b}\right)Z_0^3 + \sum_{m=1}^{\infty}\left(A_m^3 \frac{coshk_m^3 x}{coshk_m^3 b} + B_m^3 \frac{sinhk_0^3 x}{coshk_m^3 b}\right)Z_m^3, (-b < x < b, -d < z < -d_1 - h) \tag{9}$$

$$\psi_n^4 = A_0^4 e^{ik_0^4(x-b)} Z_0^4 + \sum_{m=1}^{\infty} A_m^4 e^{-k_m^4(x-b)} Z_m^4, (-b < x < \infty, -d < z < 0) \tag{10}$$

where Ψ_n^1, Ψ_n^2, Ψ_n^3, and Ψ_n^4 are the velocity potential of the n-th wave component for subregion Ω_1, Ω_2, Ω_3, and Ω_4, respectively (superscripts denote the number of subregions; A and B are unknown coefficients); and $k^{1,2,3,4}$ and $Z^{1,2,3,4}$ are the corresponding wave numbers and eigenfunctions for each subdomain, respectively.

It should be noted that the items in Equations (7) and (10) represent different modes of velocity potential. The first and second items in Equation (7) are the velocity potential of incident and reflected waves, respectively, while the infinite series are the evanescent modes existing only in the local zone near the structure. For the velocity potential of Ω_4 shown in Equation (10), the first item is the transmitted waves; while the infinite series are the evanescent modes, which attenuate quickly following the propagation of transmitted waves.

The eigenfunctions are the same for subregions Ω_1 and Ω_4:

$$Z_{nm}^{1,4} = \begin{cases} \sqrt{2} coshk_{n0}^{1,4}(z+d)/\left(d+\sigma^{-1}sinh^2 k_{n0}^{1,4} d\right)^{1/2} & m=0 \\ \sqrt{2} cosk_{nm}^{1,4}(z+d)/\left(d-\sigma^{-1}sin^2 k_{nm}^{1,4} d\right)^{1/2} & m=1,2,\cdots \end{cases} \tag{11}$$

and wave numbers can obtained from the dispersion relation:

$$\sigma = (\omega_n)^2/g = \begin{cases} k_{n0}^{1,4} tanhk_{n0}^{1,4} d & n=0 \\ -k_{nm}^{1,4} tank_{nm}^{1,4} d & n=1,2,\cdots \end{cases} \tag{12}$$

Similarly, the eigenfunctions and wave numbers for subregion Ω_2 are:

$$Z_{nm}^{2} = \begin{cases} \sqrt{2} coshk_{n0}^{2}(z+d_1)/\left(d_1+\sigma^{-1}sinh^2 k_{n0}^{2} d_1\right)^{1/2} & m=0 \\ \sqrt{2} cosk_{nm}^{2}(z+d_1)/\left(d_1-\sigma^{-1}sin^2 k_{nm}^{2} d_1\right)^{1/2} & m=1,2,\cdots \end{cases} \tag{13}$$

$$\sigma = (\omega_n)^2/g = \begin{cases} k_{n0}^{2} tanhk_{n0}^{2} d_1 & n=0 \\ -k_{nm}^{2} tank_{nm}^{2} d_1 & n=1,2,\cdots \end{cases} \tag{14}$$

and for subregion Ω_3 are:

$$Z_{nm}^{3} = \begin{cases} 1/(d-d_1-h)^{1/2} & m=0 \\ \sqrt{2} cosk_{nm}^{3}(z+d)/(d-d_1-h)^{1/2} & m=1,2,\cdots \end{cases} \tag{15}$$

$$k_{nm}^{3} = \mathrm{m}\pi/(d-d_1-h) \quad m=0,1,2\cdots \tag{16}$$

The eigenfunctions shown in Equations (11), (13) and (15) are orthogonal to others in the z-axis direction in the corresponding water depths.

2.3. Matching Conditions

The velocity potential and horizontal velocity should be continuous at the interface $x = \pm b$ with:

$$\begin{aligned} {\psi_n}^1 &= \begin{cases} {\psi_n}^2 \\ {\psi_n}^3 \end{cases}, \quad \frac{\partial {\psi_n}^1}{\partial x} = \begin{cases} \frac{\partial {\psi_n}^2}{\partial x} \\ \frac{\partial {\psi_n}^3}{\partial x} \end{cases}, \left(x=-b, \quad \begin{matrix} -d_1 \le z \le 0 \\ -d \le z \le -d_1-h \end{matrix} \right) \\ {\psi_n}^4 &= \begin{cases} {\psi_n}^2 \\ {\psi_n}^3 \end{cases}, \quad \frac{\partial {\psi_n}^4}{\partial x} = \begin{cases} \frac{\partial {\psi_n}^2}{\partial x} \\ \frac{\partial {\psi_n}^3}{\partial x} \end{cases}, \left(x=b, \quad \begin{matrix} -d_1 \le z \le 0 \\ -d \le z \le -d_1-h \end{matrix} \right) \end{aligned} \tag{17}$$

Substituting Equations (7)-(10) into Equation (17) and applying the orthogonality of the eigenfunctions, a series of integral equations can be obtained as:

$$\begin{array}{ll} \int_{-d_1}^{0} {\psi_n}^1 Z_n^2 dz = \int_{-d_1}^{0} {\psi_n}^2 Z_n^2 dz, & (x=-b) \\ \int_{-d}^{-d_1-h} {\psi_n}^1 Z_n^3 dz = \int_{-d}^{-d_1-h} {\psi_n}^3 Z_n^3 dz, & (x=-b) \\ \int_{-d_1}^{0} {\psi_n}^2 Z_n^2 dz = \int_{-d_1}^{0} {\psi_n}^4 Z_n^2 dz, & (x=b) \\ \int_{-d}^{-d_1-h} {\psi_n}^3 Z_n^3 dz = \int_{-d}^{-d_1-h} {\psi_n}^4 Z_n^3 dz, & (x=b) \\ \int_{-d}^{0} {\psi_n}^1 Z_n^1 dz = \int_{-d}^{-d_1-h} {\psi_n}^3 Z_n^1 dz + \int_{-d_1}^{0} {\psi_n}^2 Z_n^1 dz, & (x=-b) \\ \int_{-d}^{-d_1-h} {\psi_n}^3 Z_n^4 dz + \int_{-d_1}^{0} {\psi_n}^2 Z_n^4 dz = \int_{-d}^{0} {\psi_n}^4 Z_n^4 dz, & (x=b) \end{array} \tag{18}$$

Finally, the unknown coefficients A^1, A^2, B^2, A^3, B^3, and A^4 can be solved out from the 6M+6 dimensional algebraic equation series with truncating number M of the evanescent modes in the velocity potential.

2.4. Hydrodynamic Characteristics

The final complex velocity potential in each subregion can be expressed as:

$$\Phi^j(x,z,t) = -\frac{ig}{\omega Z_{00}} \sum_{n=1}^{N_f} a_n \psi_n^j e^{-i\theta_n}, Z_{00} = Z_0^1\big|_{z=0}, j = 1,\ 2,\ 3, \tag{19}$$

The reflection and transmission coefficients of the n-th wave frequency component are the coefficients $R_n = \left|A_{n0}^1\right|$ and $T_n = \left|A_{n0}^4\right|$, satisfying

$$R_n{}^2 + T_n{}^2 = 1 \tag{20}$$

to meet the conservation of wave energy in the entire fluid domain. The reflection coefficient of a focused wave group is calculated by

$$K_R = \sqrt{E_R/E_I} \tag{21}$$

where E_R and E_I are reflected and incident wave energy, respectively.

The pressure can be obtained from the velocity potential by Bernoulli's principle

$$p^j(x,z,t) = \boldsymbol{Re}\left\{-\rho \sum_{n=1}^{N_f} \frac{\partial \Phi^j}{\partial t}\right\} = \boldsymbol{Re}\left\{\sum_{n=1}^{N_f} \frac{\rho g a_n}{Z_{00}} \psi_n^j e^{-i\theta_n}\right\} \tag{22}$$

where ρ is the wave water density. The wave loads acting on a submerged plate can be calculated by integrating the pressure over the structural surface

$$F_X = \boldsymbol{Re}\left\{\int_{-d_1-h}^{-d_1} \left(p^1\big|_{x=-b} - p^4\big|_{x=b}\right) dz\right\} \tag{23}$$

$$F_Z = \boldsymbol{Re}\left\{\int_{-b}^{b} \left(-p^2\big|_{z=-d_1} + p^3\big|_{z=-d_1-h}\right) dx\right\} \tag{24}$$

$$M = \boldsymbol{Re}\left\{\int_{-b}^{b} \left(p^2\big|_{z=-d_1} - p^3\big|_{z=-d_1-h}\right) x dx + \int_{-d_1-h}^{-d_1} \left(p^1\big|_{x=-b} - p^4\big|_{x=b}\right)(z + d_1 + h) dz\right\} \tag{25}$$

where F_X and F_Z are the wave forces in the horizontal and vertical direction, while M is the overturning moment about the centroid of the plate.

Without loss of generality, the pressure and forces generated by a focused wave group with A_{max} are nondimensionalized as

$$p^* = \frac{p}{\rho g A_{max}},\ F_X{}^* = \frac{F_X}{\rho g A_{max} h},\ F_Z{}^* = \frac{F_Z}{\rho g A_{max} B},\ M^* = \frac{M}{0.5 \rho g A_{max} B^2} \tag{26}$$

3. Truncation and Validation

3.1. Truncating Effect

There are evanescent modes in the velocity potential of each subregion as shown in Equations (7)–(10). The accuracy and convergence of the analytical solution would be influenced by the truncation of the infinite series as only limited evanescent modes can be considered during implementation of the present model. The convergence of the analytical solution was checked by truncating the infinite series at $m = M$. Figure 2 shows the calculation results of the reflection coefficient, wave pressure at points P1, P2, P3, P4 as shown in Figure 1. and wave forces with different order of M for two cases with different configurations of wave structure system and incident focused wave. It can be observed that the results of both cases converge to a stable value with fluctuation less than 0.5% with 7 orders of evanescent modes. The truncating order is set as 11 in the following study with a balance between accuracy and efficiency.

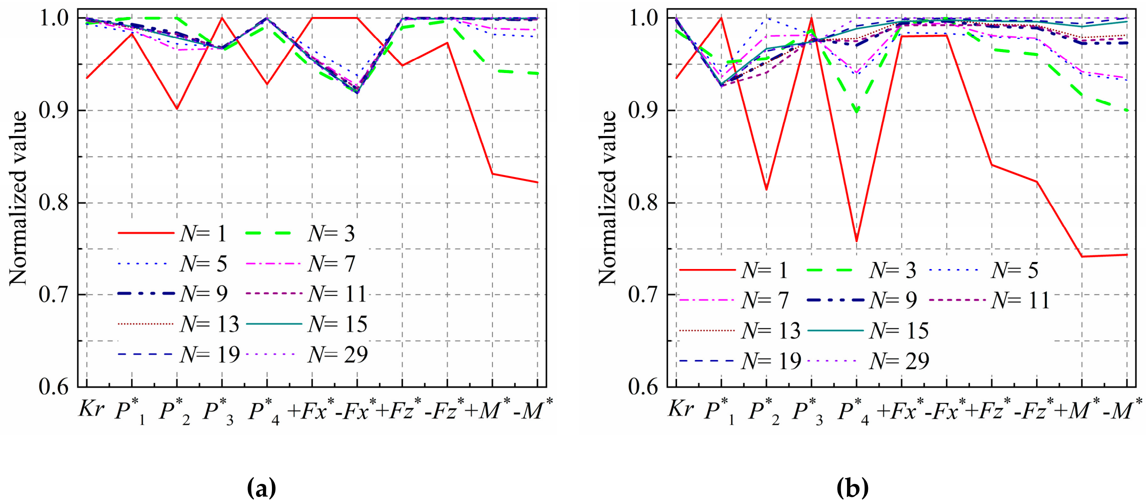

Figure 2. Truncating effect of pressure and wave forces acting on the submerged plate: (**a**) Case 1: $k_P d = 1.12$, $A_{max}/d = 0.14$, $d_1/d = 0.25$, $h/d = 0.1$, $B/d = 2$; (**b**) Case 2: $k_P d = 0.79$, $A_{max}/d = 0.1$, $d_1/d = 0.16$, $h/d = 0.03$, $B/d = 1.5$.

3.2. Comparison with Existing Results

Following the analytical formulation presented in Section 2, the solution of focused wave actions is based on the results of monochronic wave action. The results of monochronic wave action from the present model can be validated by existing studies. Figure 3 shows a comparison of reflection coefficient and, horizontal and vertical wave forces between the present model and the model in reference [36]. Kojima, et al. [36] setup an analytical model of wave action on a submerged horizontal plate above flat seabed using the eigenfunction expansion method and conducted a series of wave flume tests to validate it. It can be seen from Figure 3 that the present model is in good agreement with the solution of Kojima, et al. [36], except for a slight difference in horizontal wave force around d/L_W ranging from 0.15 to 0.35. Moreover, wave forces calculated by the present model are quite consistent with test data. Due to the nonlinear factors of water overtopping and wave breaking, which cannot be considered in the present model, differences can be observed for vertical wave forces around 0.15 and 0.3.

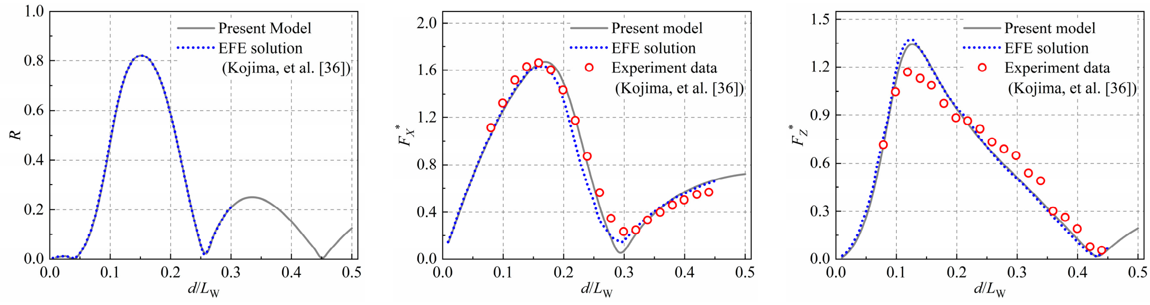

(a) (b) (c)

Figure 3. Comparison of (**a**) reflection and (**b**,**c**) wave loads on submerged plate between present study and result of Kojima, et al. [36].

3.3. Limiting Cases

With the validated analytical model, two limiting cases are considered. The first one is wave motion over submerged thin plates. When the structural height of the submerged plate is set as a small value, it transforms into a thin plate. Patarapanich and Cheong [25] conducted an experiment in the wave flume to check the reflection of a submerged thin plate. This limiting case was also employed to validate their analytical solution of wave action on a submerged breakwater formed by an upper porous plate and a lower solid plate [37]. The configurations of the limiting case are $d_1/d = 0.3$ and $d/L = 0.2$. In the present model of this case, the relative plate thickness is set as a small value, $h/d = 0.01$, to meet the assumption of thin plate. The results of reflection and transmission coefficients of present model, Liu, et al. [37], and an experiment [25] are compared in Figure 4. The present model can reasonably converge to the limiting case without obvious difference and give a reasonable prediction about the reflection and transmission coefficients, similar to the theoretical results of Liu, et al. [37]. The overall difference between the analytical solution and the experimental data can be attributed to wave energy dissipation during wave interaction with the submerged plate, which is not included in the analytical model.

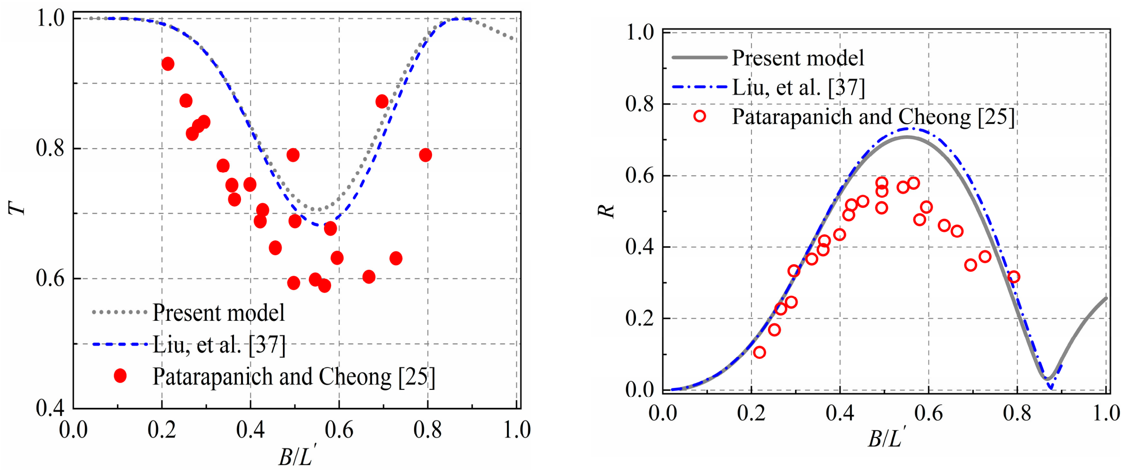

(a) (b)

Figure 4. Comparison between the present method and the existing results [25,37] of thin plate: (**a**) Transmission; (**b**) Reflection.

When the submerged plate is located on the seabed, it transforms into a bottom obstacle. The bottom obstacle, which is a simplification of various bottom topographies, plays an important role in determination of wave climate [38]. Cho, et al. [38] conducted an experiment to study the reflection of bottom obstacles and compared the test data with theoretical results. By setting the gap under the plate as a small value, $S/d = 0.01$, the present model can investigate the wave action on a bottom obstacle. The configurations of the limiting case are $d_1/d = 0.5$, $h/d = 0.49$, and $B/d = 0.5$. Figure 5 shows a comparison of reflection coefficients obtained by the present model and Cho, et al. [38]. It can be observed from Figure 5 that both the present model and the analytical model built by Cho, et al. [38] can give a reasonable estimation of wave reflection led by a bottom obstacle for small k_0d. However, the present model underestimates the reflection coefficient for k_0d in the range of 2.5 to 4.0, which means the bottom obstacle could lead to more sever reflection than predicted for short waves. It should be noted that the present model gives a better prediction around $k_0d = 1.0$ than Cho, et al. [38], because there is a tiny gap between the submerged obstacle and the seabed that would transmit wave energy.

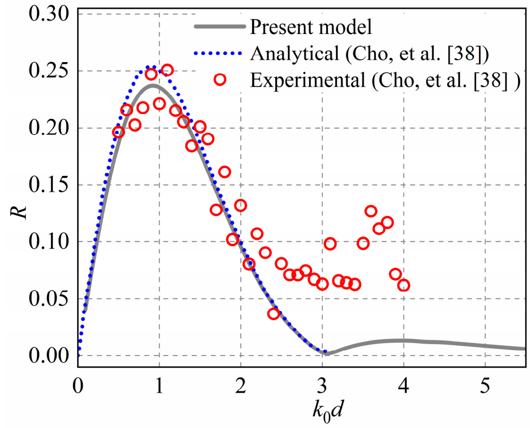

Figure 5. Comparison between present method and existing results [38] of rectangular obstacle on seabed.

4. Results and Discussion

With specific focusing on time and location, the initial phase of every wave component can be determined and the time series of pressure and forces acting on a plate during a focused wave can be obtained. Figure 6 shows the calculated time series of pressure and forces acting on a submerged plate during a focused wave with the focusing point at the center of the plate ($x_b = 0.0\ m$) and focusing time $t_b = 5.0\ s$. The pressure at four locations shown in Figure 1 are plotted in Figure 6. It can be seen from Figure 6. that the maximum pressure acting on the offshore side surface is about two times that on the onshore side surface. The maximum pressure on the offshore and onshore side surfaces occurs at almost same time. The pressure acting on the top is larger and earlier than on the bottom of the plate as shown in Figure 6.

It is well known that wave loads acting on structures are influenced by the wave property of incident waves and the configuration of the wave structure system. It can be expressed as:

$$F = f\left(\rho, g, A_{max}, L_p, d, d_1, h, B\right) \tag{27}$$

where F can be forces F_X, F_Z and M_Y or pressure $P(x,z)$. Following Equation (26), the dimensionless forces depend on a set of variables:

$$(p^*, F_X{}^*, F_Z{}^*, M^*) = f\left(\frac{d}{L_P}, \frac{d_1}{d}, \frac{h}{d}, k_P B\right) \tag{28}$$

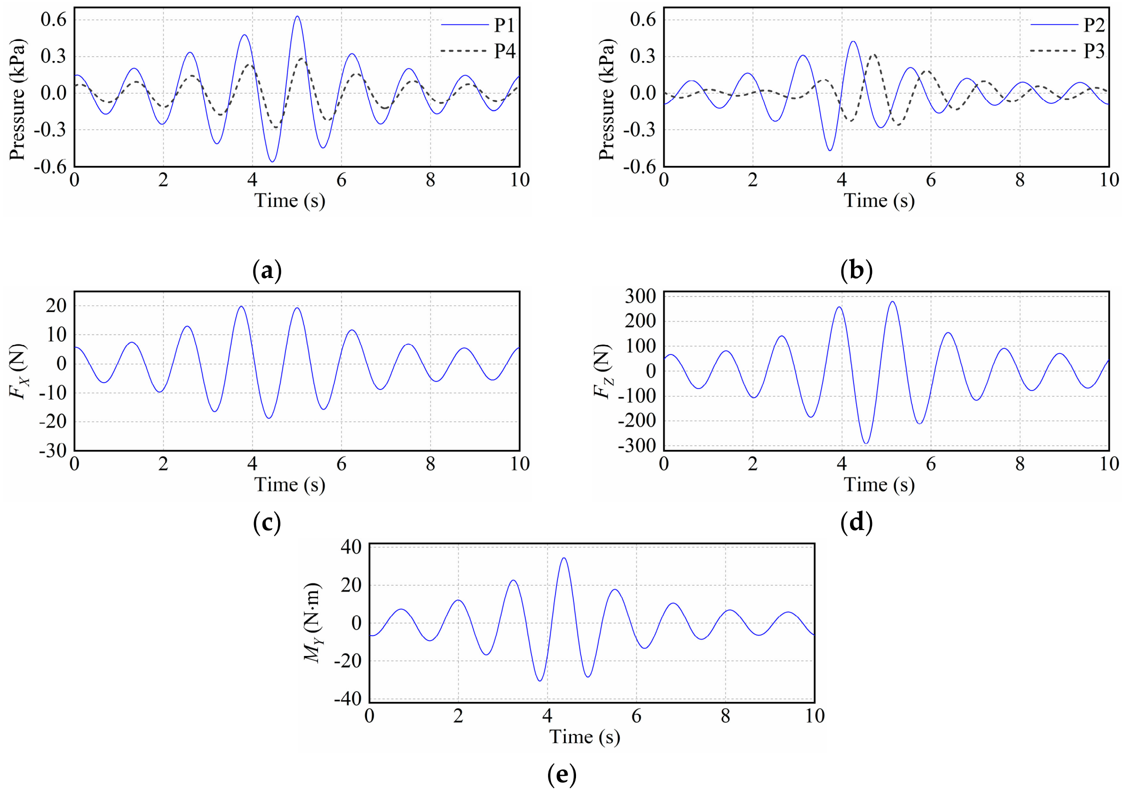

Figure 6. Typical time series of (**a**,**b**) hydrodynamic pressure and (**c**–**e**) wave forces: $k_P d = 1.12$, $A_{max}/d = 0.25$, $d_1/d = 0.25$, $h/d = 0.1$, $B/d = 2$. (**a**) Pressure at location P1 and P4; (**b**) Pressure at location P2 and P3; (**c**) Horizontal wave force; (**d**) Vertical wave force; (**e**) Overturning moment.

To check the influence of the configuration of wave-structure, parametric analysis is carried out based on the present model in this section. The maximum of wave forces in both positive and negative during a focused wave with the focusing location at the center of plate ($x_b = 0.0$ m) is discussed in the following.

4.1. Effect of Peak Frequency

As indicated in Equation (3), wave spectrum is employed to determine the amplitude of wave components of the focused wave group, which means the elevation of the focused wave group would be influenced by the parameters of the wave spectrum. The peak frequency of the wave spectrum changes with different zones. Figure 7 shows the influence of peak frequency on the reflection coefficients and wave forces during the focused wave group. The ratio of water depth to wave length L_P corresponding to the peak frequency in the offshore subregion is used to evaluate the influence of the peak frequency. The other parameters are $d_1/d = 0.25$ and $h/d = 0.25$. Figure 7 shows the results of reflection coefficients and wave forces about the ratio of water depth to wave length d/L_P. It can be seen from Figure 7 that the reflection coefficient first increases and then decreases gradually with d/L_P for short plate $B/d = 1.5$. For long plates, there are some fluctuations after decreasing. The maximum reflection occurs at different ratios of water depth to wave length for different wave forces sharing a similar tendency about d/L_P with the reflection coefficient. It can be seen that the submerged plate experiences larger downward vertical forces during focused wave action rather than upward forces. The focused wave group with low peak frequency can generate larger wave forces on long submerged plates.

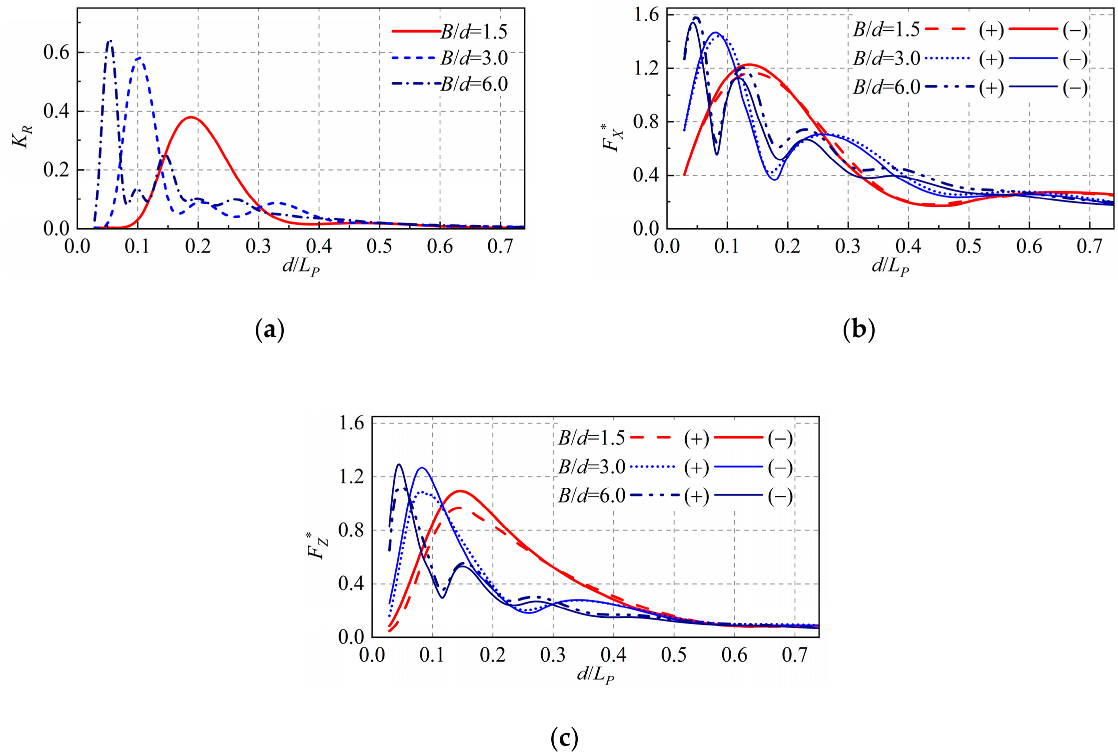

Figure 7. Variations of reflection coefficients and wave forces about the ratio of water depth to wave length d/L_P with different relative breadth: (**a**) reflection coefficient, (**b**) horizontal force and (**c**) vertical force.

4.2. Effect of Submergence

For surface gravity wave action, submergence would be an important factor for submerged structures. The change of reflection coefficient about relative submergence d_1/d is plotted in Figure 8. The parameter W/d was taken as 1.5 and h/d as 2.5. The reflection coefficient and wave forces show different tendencies about d_1/d under focused wave with different peak frequencies. For the focused wave with low peak difference, the reflection coefficient first decreases, then increases with a peak around $d_1/d = 0.18$, followed by gradual decrease. However, the reflection coefficient drops quickly and remains quite small with the change of relative submergence. The horizontal wave force is closely related to wave reflection. Strong reflection leads to a large horizontal force acting on submerged plates. It is obvious that the horizontal force almost keeps stable when the plate is submerged deeply enough, e.g., $d_1/d = 0.3$ for a focused wave with $d/L_P = 0.338$.

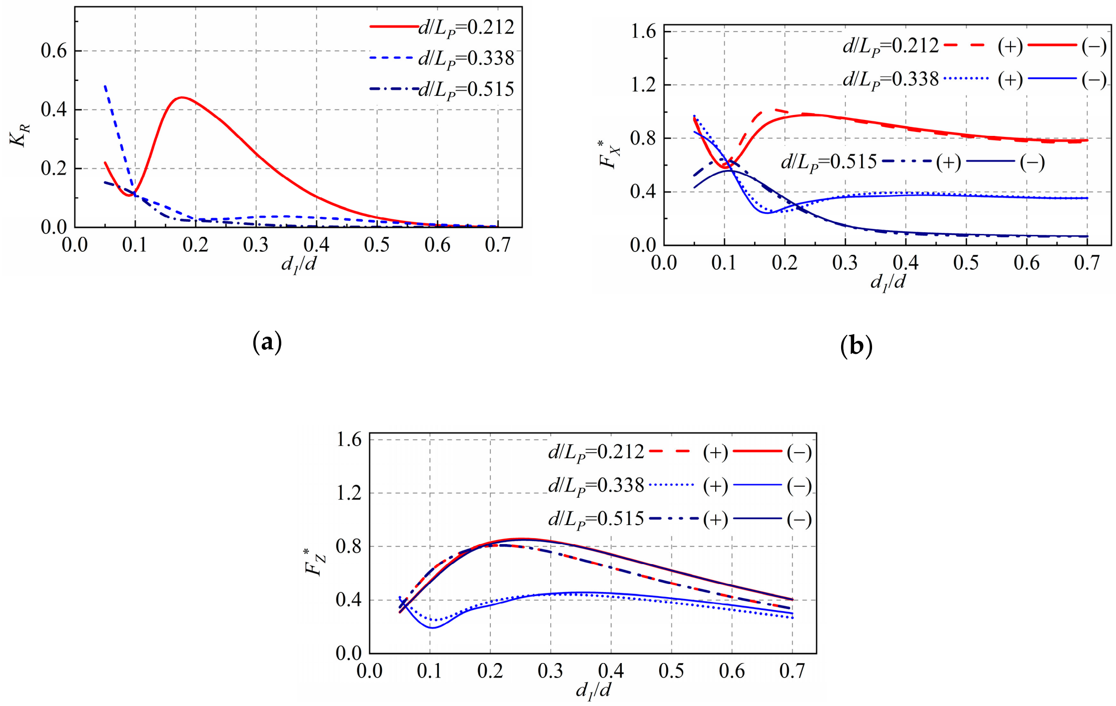

(**a**) (**b**) (**c**)

Figure 8. Variations of reflection coefficients and wave forces about dimensionless submergence d_1/d with different peak wave length (**a**) reflection coefficient, (**b**) horizontal force and (**c**) vertical force.

4.3. Effect of Structural Configuration

Figure 9 shows the results of reflection coefficients and wave forces about dimensionless structural breadth $k_P B$. Focusing on the influence of breadth, the other parameters are kept constant as $d_1/d = 0.25$ and $h/d = 0.25$. With the increase of $k_P B$, the reflection coefficient increases gradually and peaks around $k_P B = 2.0$, then drops to near 0.05 around 3.0. A similar tendency can be found for horizontal and vertical wave forces but with a peak in the range of $k_P B = 1.5$ to 2.0. It can be observed that the amplitude of negative horizontal wave forces is larger than the maximum positive horizontal wave force for $k_P B > 2.0$. A focused wave with high peak frequency can generates more vertical wave force on short plates with $k_P B < 0.7$ in comparison with a focused wave with low peak frequency, while it is the opposite for longer plates.

Figure 10 shows the reflection coefficients and wave forces for submerged plates with different structural height h/d but constant width $W/d = 1.5$ under submergence $d_1/d = 0.15$. It can be observed from Figure 10. that the reflection coefficient decreases steadily with the increased structural height for a focused wave with low peak frequency. When d/L_P changes to 0.338, the reflection coefficient almost remains constant at a small value and is not influenced by structural height. The horizontal wave force in the negative and positive directions, generated by a focused wave with $d/L_P = 0.125$, shows different tendencies about d/L_P. The maximum negative horizontal wave force increases slightly but declines steadily with d/L_P increasing from 0.01 to 0.71. Vertical force is seldom influenced by a change of structural height, especially for focused wave with high peak frequency.

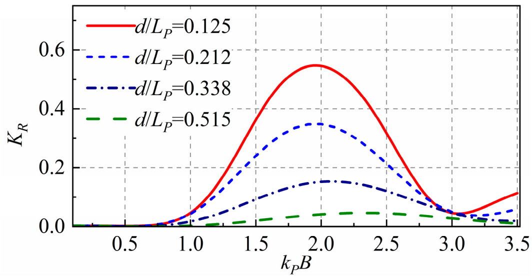

(**a**)

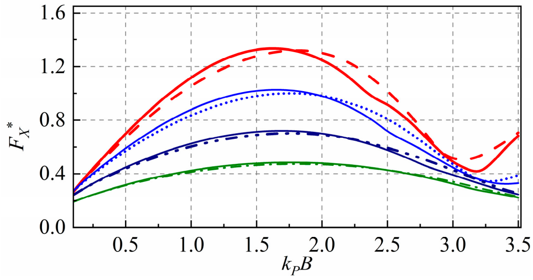

(**b**)

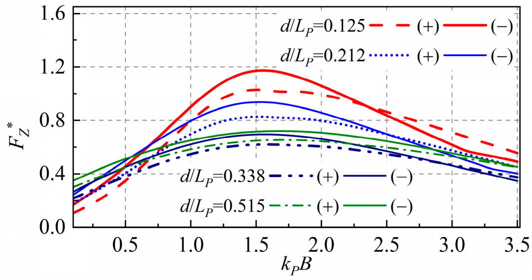

(**c**)

Figure 9. Variations of reflection coefficients and wave forces about dimensionless breadth $k_P B$ with different peak wave length (**a**) reflection coefficient, (**b**) horizontal force and (**c**) vertical force.

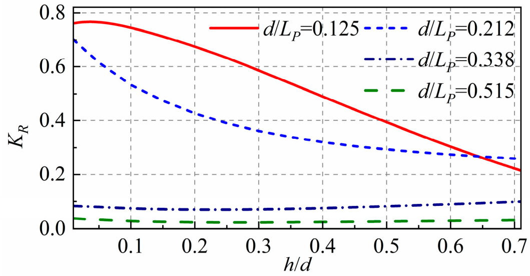

(**a**)

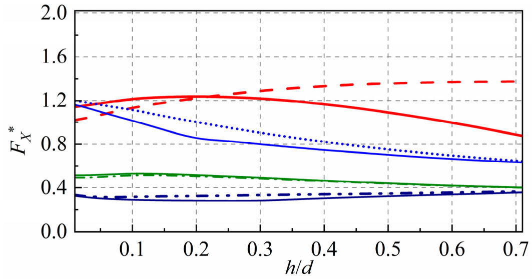

(**b**)

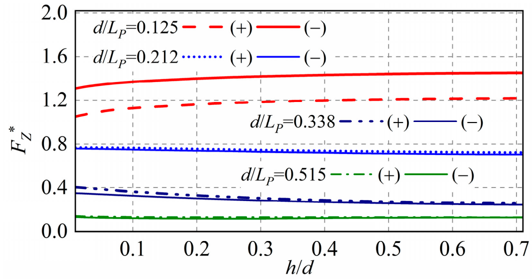

(**c**)

Figure 10. Variations of reflection coefficients and wave forces about dimensionless structural height h/d with different peak wave length (**a**) reflection coefficient, (**b**) horizontal force and (**c**) vertical force.

5. Conclusions

In this paper, a general solution of focused wave action on a submerged plate was obtained based on potential flow theory and matching eigenfunction methods. The validated analytical model can estimate the wave forces acting on a submerged plate in comparison with existing experimental studies. By setting the structural height of the plate and the gap under the plate as small values, the present model turned it into a thin plate and bottom obstacle, and it was checked with hydrodynamic experiments. With the validated analytical model, a detailed parametric study was conducted to investigate the effects of wave properties and the configuration of the wave structure system on the hydrodynamic performance of submerged plates. The result shows that the reflection coefficients and wave forces are sensitive to the peak frequency of focused wave and structural breadth. The submergence of the plate significantly influences its hydrodynamic performance in a relatively small range of $d_1/d < 0.2$. However, the wave forces acting on plates are seldom changed by structural height.

In this paper, the accuracy and convenience of the analytical model was confirmed for investigating wave forces generated by focused waves, and it could be employed as a preliminary tool in engineering design. However, nonlinear factors, such as high-order harmonics and wave breaking, cannot be considered by the present model. The former could be treated in a full nonlinear analytical model, but wave breaking needs Navier–Stokes equations solver to take viscosity into consideration. Furthermore, specific physical model tests with focused wave generation should be conducted in the future to validate the analytical or numerical model.

Author Contributions: Q.F. and C.Y. derived the analytical model and conducted all the calculations. Q.F. wrote the original draft. A.G. reviewed the paper and contributed to the parametric analysis.

Funding: This research was funded by the National Natural Science Foundation of China with grant number 51808172 and 51725801, and the China Postdoctoral Science Foundation project with grant number 2018M641833. This work was also partially supported by open funding from the Key Laboratory of Coastal Disasters and Defense of the Ministry of Education with grant number 201802.

Conflicts of Interest: The authors declare no conflict of interest.

References

1. Dysthe, K.; Krogstad, H.E.; Muller, P. Oceanic rogue waves. *Annu. Rev. Fluid. Mech.* **2008**, *40*, 287–310. [CrossRef]
2. Chien, H.; Kao, C.C.; Chuang, L.Z.H. On the characteristics of observed coastal freak waves. *Coast. Eng. J.* **2002**, *44*, 301–319. [CrossRef]
3. Kharif, C.; Pelinovsky, E. Physical mechanisms of the rogue wave phenomenon. *Eur. J. Mech. B Fluids* **2003**, *22*, 603–634. [CrossRef]
4. Chaplin, J.R. On Frequency-Focusing Unidirectional Waves. *Int. J. Offshore Polar Eng.* **1996**, *6*, 131–137.
5. Sriram, V.; Schlurmann, T.; Schimmels, S. Focused wave evolution using linear and second order wavemaker theory. *Appl. Ocean. Res.* **2015**, *53*, 279–296. [CrossRef]
6. Ning, D.Z.; Zang, J.; Liu, S.X.; Eatock Taylor, R.; Teng, B.; Taylor, P.H. Free-surface evolution and wave kinematics for nonlinear uni-directional focused wave groups. *Ocean. Eng.* **2009**, *36*, 1226–1243. [CrossRef]
7. Chaplin, J.; Rainey, R.; Yemm, R. Ringing of a vertical cylinder in waves. *J. Fluid Mech.* **1997**, *350*, 119–147. [CrossRef]
8. Fitzgerald, C.; Taylor, P.H.; Taylor, R.E.; Grice, J.; Zang, J. Phase manipulation and the harmonic components of ringing forces on a surface-piercing column. *Proc. R. Soc. A Math. Phys. Eng. Sci.* **2014**, *470*, 20130847. [CrossRef]
9. Chen, L.; Zang, J.; Taylor, P.H.; Sun, L.; Morgan, G.; Grice, J.; Orszaghova, J.; Ruiz, M.T. An experimental decomposition of nonlinear forces on a surface-piercing column: Stokes-type expansions of the force harmonics. *J. Fluid Mech.* **2018**, *848*, 42–77. [CrossRef]
10. Deng, Y.; Yang, J.; Zhao, W.; Li, X.; Xiao, L. Freak wave forces on a vertical cylinder. *Coast. Eng.* **2016**, *114*, 9–18. [CrossRef]

11. Ghadirian, A.; Bredmose, H.; Dixen, M. Breaking phase focused wave group loads on offshore wind turbine monopiles. In Proceedings of the Science of Making Torque from Wind (TORQUE 2016), München, Germany, 5–7 October 2016.
12. Buldakov, E.; Stagonas, D.; Simons, R. Extreme wave groups in a wave flume: Controlled generation and breaking onset. *Coast. Eng.* **2017**, *128*, 75–83. [CrossRef]
13. Gao, N.; Yang, J.; Tian, X.; Li, X. A numerical study on the nonlinear effects in focused wave modelling and forces on a semi-submerged horizontal cylinder. *Ships Offshore Struct.* **2016**, *12*, 474–485. [CrossRef]
14. Gao, N.; Yang, J.; Zhao, W.; Li, X. Numerical simulation of deterministic freak wave sequences and wave-structure interaction. *Ships Offshore Struct.* **2016**, *11*, 802–817. [CrossRef]
15. Westphalen, J.; Greaves, D.M.; Williams, C.J.K.; Hunt-Raby, A.C.; Zang, J. Focused waves and wave–structure interaction in a numerical wave tank. *Ocean. Eng.* **2012**, *45*, 9–21. [CrossRef]
16. Weller, S.D.; Stallard, T.J.; Stansby, P.K. Experimental measurements of the complex motion of a suspended axisymmetric floating body in regular and near-focused waves. *Appl. Ocean. Res.* **2013**, *39*, 137–145. [CrossRef]
17. Zhao, X.; Hu, C. Numerical and experimental study on a 2-D floating body under extreme wave conditions. *Appl. Ocean. Res.* **2012**, *35*, 1–13. [CrossRef]
18. Banks, M.; Abdussamie, N. The response of a semisubmersible model under focused wave groups: Experimental investigation. *J. Ocean. Eng. Sci.* **2017**, *2*, 161–171. [CrossRef]
19. Deng, Y.; Yang, J.; Zhao, W.; Xiao, L.; Li, X. Surge motion of a semi-submersible in freak waves. *Ships Offshore Struct.* **2017**, *12*, 443–451. [CrossRef]
20. Suchithra, N.; Koola, P.M. A study of wave impact of horizontal slabs. *Ocean. Eng.* **1995**, *22*, 687–697. [CrossRef]
21. Lu, X.; Kumar, P.; Bahuguni, A.; Wu, Y. A CFD Study of Focused Extreme Wave Impact on Decks of Offshore Structures. In Proceedings of the ASME 2014 33rd International Conference on Ocean, Offshore and Arctic Engineering, San Francisco, CA, USA, 8–13 June 2014.
22. Qin, H.; Tang, W.; Xue, H.; Hu, Z. Numerical study of nonlinear freak wave impact underneath a fixed horizontal deck in 2-D space. *Appl. Ocean. Res.* **2017**, *64*, 155–168. [CrossRef]
23. Qin, H.; Tang, W.; Hu, Z.; Guo, J. Structural response of deck structures on the green water event caused by freak waves. *J. Fluids Struct.* **2017**, *68*, 322–338. [CrossRef]
24. Cheng, Y.; Ji, C.; Ma, Z.; Zhai, G.; Oleg, G. Numerical and experimental investigation of nonlinear focused waves-current interaction with a submerged plate. *Ocean. Eng.* **2017**, *135*, 11–27. [CrossRef]
25. Patarapanich, M.; Cheong, H.-F. Reflection and transmission characteristics of regular and random waves from a submerged horizontal plate. *Coast. Eng.* **1989**, *13*, 161–182. [CrossRef]
26. Karmakar, D.; Guedes Soares, C. Wave Motion Control Over Submerged Horizontal Plates. *J. Offshore Mech. Arct. Eng.* **2018**, *140*, 031101. [CrossRef]
27. Wang, K.-H.; Shen, Q. Wave motion over a group of submerged horizontal plates. *Int. J. Eng. Sci.* **1999**, *37*, 703–715. [CrossRef]
28. Yu, X. Functional performance of a submerged and essentially horizontal plate for offshore wave control: A review. *Coast. Eng. J.* **2002**, *44*, 127–147. [CrossRef]
29. Liu, Y.; Faraci, C. Analysis of orthogonal wave reflection by a caisson with open front chamber filled with sloping rubble mound. *Coast. Eng.* **2014**, *91*, 151–163. [CrossRef]
30. Faraci, C.; Scandura, P.; Foti, E. Reflection of sea waves by combined caissons. *J. Waterw. Port. Coast. Ocean. Eng.* **2014**, *141*, 04014036. [CrossRef]
31. Tromans, P.S.; Anaturk, A.R.; Hagemeijer, P. A New Model for the Kinematics of Large Ocean Waves-Application as a Design Wave. In Proceedings of the First International Offshore and Polar Engineering Conference, Edinburgh, UK, 11–16 August 1991; pp. 64–71.
32. Vyzikas, T.; Stagonas, D.; Buldakov, E.; Greaves, D. The evolution of free and bound waves during dispersive focusing in a numerical and physical flume. *Coast. Eng.* **2018**, *132*, 95–109. [CrossRef]
33. Goda, Y. A comparative review on the functional forms of directional wave spectrum. *Coast. Eng. J.* **1999**, *41*, 1–20. [CrossRef]
34. Cheong, H.F.; Shankar, N.J.; Nallayarasu, S. Analysis of submerged platform breakwater by Eigenfunction Expansion Method. *Ocean. Eng.* **1996**, *23*, 649–666. [CrossRef]

35. Dong, J.; Wang, B.; Zhao, X.; Liu, H. Wave Forces Exerted on a Submerged Horizontal Plate over an Uneven Bottom. *J. Eng. Mech.* **2018**, *144*, 04018030. [CrossRef]
36. Kojima, H.; Yoshida, A.; Nakamura, T. Linear and nonlinear wave forces exerted on a submerged horizontal plate. In Proceedings of the 24th International Conference on Coastal Engineering, Kobe, Japan, 23–28 October 1994; pp. 1312–1326.
37. Liu, Y.; Li, Y.C.; Teng, B.; Dong, S. Wave motion over a submerged breakwater with an upper horizontal porous plate and a lower horizontal solid plate. *Ocean. Eng.* **2008**, *35*, 1588–1596. [CrossRef]
38. Cho, Y.-S.; Lee, J.-I.; Kim, Y.-T. Experimental study of strong reflection of regular water waves over submerged breakwaters in tandem. *Ocean. Eng.* **2004**, *31*, 1325–1335. [CrossRef]